BLIND HYPERSPECTRAL INPAINTING VIA JOHN ELLIPSOID

Chia-Hsiang Lin[†]*, and Yangrui Liu*[†]

[†]Department of Electrical Engineering, National Cheng Kung University, Tainan, Taiwan
Email: chiahsiang.steven.lin@gmail.com; q36083030@gs.ncku.edu.tw

ABSTRACT

Hyperspectral inpainting (HI) is a signal processing technique for recovering the complete hyperspectral imaging data cube from its incompletely acquired version. Some benchmark methods either rely on big data or the plug-and-play learning strategy. In this paper, we introduce John ellipsoid (JE), a key topology in functional analysis, to design a *blind* HI algorithm. JE criterion holds strong endmember identifiability like the well known (non-convex) minimum-volume simplex criterion in hyperspectral remote sensing, but just requires solving a convex optimization problem bringing it an advantage in computational aspect. As revealed in recent literature, comparing to widely adopted simplex topology, JE is robust against both low purity of hyperspectral data and ill-conditioned endmember matrix. Such robustness does bring us advantage in HI performance, as illustrated by experimental results on benchmark dataset.

***Index Terms*—** Hyperspectral image, hyperspectral inpainting, John ellipsoid, blind signal processing, functional analysis

1. INTRODUCTION

Hyperspectral image (HSI) has found its broad applications, including change detection, material identification, land classification, etc. During the acquisition and/or transmission of HSI, the data are quite often corrupted or incompletely observed, leading to some dead pixels or low-quality bands. Large areas of dead pixels in consecutive bands will seriously degrade the effectiveness of HSI applications. In order to ensure the quality of service in various HSI applications, it's indispensable to restore the incomplete data, hopefully under an fully unsupervised learning framework.

In recent years, several high-performance hyperspectral inpainting (HI) methods have been proposed, as reviewed hereinafter. It is well known that HSI data is highly correlated in both frequency domain and spatial domain, thereby making the low-rank modeling and the total variation regularization popularly adopted in numerous HI methods; see, e.g., [1, 2]. For example, the method proposed in [2], termed local low-rank matrix recovery regularized by spatial-spectral total variation (LLRSSTV), exploits the low-rankness of local structure, and captures the smoothness of global structure based on a spatial total variation term. On the other hand, the technique of source separation has also exploited by some HI methods [3, 4], such as the unmixing based denoising/inpainting (UBD) method proposed in [3]. This kind of method may also pick up pure pixels manually or automatically, followed by some typical linear unmixing algorithm to compute the corresponding representation coefficients. However, the required pure pixel assumption is commonly violated in remotely acquired HSI data, besides the spectral variation issue [5]. Finally, the fast hyperspectral image inpainting (FastHyIn) method [6] employs the self-similarity regularization under a linear mixing model. FastHyIn encourages solutions with similarity between nonlocal patches in the eigenspace, which in turn ensures the self-similarity structure in the restored HSI. However, FastHyIn does not define the self-similarity prior explicitly [7], making it rely on the plug-and-play learning that has no convergence guarantee in general.

In this work, we attack the HI problem using John ellipsoid in functional analysis. John ellipsoid has revealed its fundamental role in hyperspectral analysis as can be seen in recent literature [8]. Unlike the widely used simplex topology in hyperspectral remote sensing [9], which amounts to non-convex NP-hard problem, computing the John ellipsoid is a convex optimization problem [8], and such convexity is proven to be critical in separating heav-

This work is funded partly by the Young Scholar Fellowship Program (Einstein Program) of Ministry of Science and Technology (MOST) in Taiwan, under Grant MOST 108-2636-E-006-012; and partly by the Higher Education Sprout Project of Ministry of Education (MOE) to the Headquarters of University Advancement at National Cheng Kung University (NCKU).

ily mixed hyperspectral data [8]. Furthermore, in most hyperspectral scenes, the material signatures (endmembers) would be quite similar to each other, leading to a high condition number of the endmember matrix. As investigated in very recent machine learning literature [10], John ellipsoid is known to be able to elegantly handle such ill-conditioned scenarios. Note that the convex John ellipsoid criterion [8] and the non-convex simplex criterion [9] surprisingly hold the same sufficient endmember identifiability condition [8, 11, 12]. These fundamental improvements motivate us to employ John ellipsoid into the HI study. As can be seen from some experimental evidence, John ellipsoid indeed yields superior HI results.

Notations: $\mathcal{I}_Z \triangleq \{1,\ldots,Z\}$ for a given positive integer Z. $\mathrm{vol}(\mathcal{S})$ denotes the volume of a measurable set $\mathcal{S}$. $\mathrm{conv}\mathcal{S}$ denotes the convex hull of the set $\mathcal{S}$ [13]. $\mathbf{1}_n$ is the n-dimensional all-one vector. $\mathbb{R}^n$ is the n-dimensional Euclidean space, and $\mathbb{R}^{m\times n}$ is the $(m\times n)$-dimensional real-valued matrix space. $\mathbb{R}^n_+$ is the non-negative orthant of $\mathbb{R}^n$, and $\mathbb{R}^{m\times n}_+$ is the set of $m\times n$ matrices with all entries being non-negative. $\|\cdot\|_1$, $\|\cdot\|_2$ and $\|\cdot\|_F$ denote ℓ_1-norm, ℓ_2-norm and Frobenius norm, respectively.

2. JOHN ELLIPSOID BASED HI METHOD

As HSI can be conveniently represented by arranging its pixels into columns of a matrix $\boldsymbol{X}\in\mathbb{R}^{M\times L}$, where M (resp., L) is the number of spectral bands (resp., pixels). In practice, $\boldsymbol{X}$ may not be completely acquired or observed; let $\overline{\boldsymbol{\Omega}}\subseteq\{(m,\ell)\mid m\in\mathcal{I}_M,\ \ell\in\mathcal{I}_L\}$ denote the set of indices of those missing data. The hyperspectral inpainting problem is then to recover $\boldsymbol{X}$ from the remaining observed data $\{[\boldsymbol{X}]_{m,\ell}\mid(m,\ell)\in\boldsymbol{\Omega}\}$, where $\boldsymbol{\Omega}\triangleq\{(m,\ell)\mid m\in\mathcal{I}_M,\ \ell\in\mathcal{I}_L\}\backslash\overline{\boldsymbol{\Omega}}$ is the set of indices of those successfully acquired/observed data.

Let $\boldsymbol{A}=[\boldsymbol{a}_1,\ldots,\boldsymbol{a}_N]\in\mathbb{R}^{M\times N}$ be the endmember matrix, whose nth column $\boldsymbol{a}_n$ is the spectral signature (endmember) of the nth material, where N is number of materials (presented in the HSI $\boldsymbol{X}$) that can be blindly estimated by information-theoretic minimum description length (MDL) criterion; see [14] for a parameter-tuning-free order-selection method. Each column of $\boldsymbol{X}=[\boldsymbol{x}_1,\ldots,\boldsymbol{x}_L]$ representing a pixel can then be modeled as a linear combination of the signatures, i.e., $\boldsymbol{x}_\ell=\sum_{n=1}^N S_{n,\ell}\boldsymbol{a}_n,\ \forall\ell\in\mathcal{I}_L$, which can be concisely written as $\boldsymbol{X}=\boldsymbol{A}\boldsymbol{S}$ with $\boldsymbol{S}=[S_{n,\ell}]\in\mathbb{R}^{N\times L}$ being the abundance matrix [15]. Therefore, the HI problem becomes estimating $\boldsymbol{A}$ and $\boldsymbol{S}$, respectively done next, from the available information in $\{[\boldsymbol{X}]_{m,\ell}\mid(m,\ell)\in\boldsymbol{\Omega}\}$.

As reported in recent imaging sciences litarature [8],

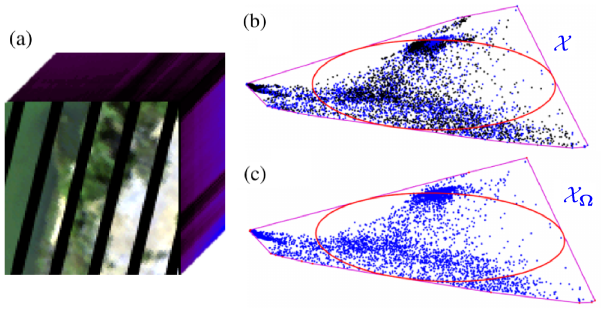

Fig. 1. A benchmark HSI seriously corrupted by stripes is illustrated in (a). Its 2-D visualization, together with the John elliposid corresponding to $\mathcal{X}$, is displayed in (b). After removing the stripe-corrupted pixels (i.e., black dots in(b)), the John ellipsoid corresponding to the remaining complete pixels in $\mathcal{X}_{\boldsymbol{\Omega}}$ (marked by blue dots) remains almost unchanged, as displayed in (c).

the topology of John ellipsoid can be used to perfectly recover signatures in $\boldsymbol{A}$ under a very mild sufficient condition on the data purity $\gamma\in(0,1]$ (defined in [11,12])—to get a sense, John ellipsoid requires just "$\gamma>\frac{1}{\sqrt{N-1}}$", though typical endmember extraction algorithms (EEAs) require "$\gamma=1$" that is equivalent to the pure-pixel assumption [11, 12].

John ellipsoid $\mathcal{E}^\star$ is the maximum-volume ellipsoid inscribed in the data convex hull, which can be explicitly formulated as the following optimization problem:

$$\mathcal{E}^\star=\arg\max_{\mathcal{E}\subseteq\mathrm{conv}\{\boldsymbol{x}_1,\ldots,\boldsymbol{x}_L\}=\mathrm{conv}\mathcal{X}}\mathrm{vol}(\mathcal{E}),\qquad(1)$$

from which $\boldsymbol{A}$ can be computed either by a simple affine mapping [8, Corollary 1] or by regular-simplex fitting in a transformed space [10, Proposition 2]. Due to space limitation, we refer readers to [8, 10] for how to obtain $\boldsymbol{A}$ from the John ellipsoid $\mathcal{E}^\star$.

At this moment, one would just need to keep in mind that, unlike the *non-convex* Craig's minimum-volume simplex EEA criterion [9], John's maximum-volume ellipsoid criterion (1) can be solved as a conic program that is *convex* [8].[1] Most importantly, such convexity has been theoretically and experimentally proven to be essential in unmixing heavily mixed hyperspectral data [8].

Though there are fundamental advantages of John

[1] As reported in the seminal IEEE WHISPERS paper [16], the Craig simplex based EEA algorithm (i.e., the simplex identification via split augmented Lagrangian (SISAL)) cannot *equivalently* reformulate the simplex volume into a convex formula since the parameter domain cannot be restricted on the positive definite (PD) cone; see [16, Page 2]. Very beautifully, the ellipsoid volume can be defined on the PD cone, allowing us to formulate the ellipsoid volume directly as a convex formulation *without approximation* [8, 10].

ellipsoid, such as robustness against the high condition number of $\boldsymbol{A}$ (e.g., caused by very similar signatures) [10] and the convexity of the criterion (that allows successful unmixing of heavily mixed signatures) [8], the criterion (1) is not directly applicable for HI because some pixels $\boldsymbol{x}_\ell$ are not completely observed. Fortunately, this turns out to be a minor issue, as discussed below, ever for a challenging HI scenario (cf. Figure 1). Specifically, empirical experience suggests that John ellipsoid can be very well approximated by

$$\mathcal{E}^\star \approx \arg \max_{\mathcal{E} \subseteq \text{conv}\mathcal{X}_{\boldsymbol{\Omega}}} \text{vol}(\mathcal{E}), \tag{2}$$

where $\mathcal{X}_{\boldsymbol{\Omega}} \subset \mathcal{X} \triangleq \{\boldsymbol{x}_1, \ldots, \boldsymbol{x}_L\}$ is the set of completely acquired pixels.

To get a sense, we illustrate the idea using an HSI with $N = 3$ endmembers for the purpose of easy visualization, in Figure 1(a), where a benchmark HSI containing serious stripes (more than 36% dead pixels) is displayed [17, 18]. This HSI data is visualized by projecting each pixel vector onto a 2-dimensional space computed by PCA, as shown in Figure 1(b), where dead pixels (resp., complete pixels) are marked by black dots (resp., blue pixels), and the data convex hull conv$\mathcal{X}$ is outlined by the purple polytope; the John ellipsoid of the complete HSI is then shown as the red ellipsoid. Remarkably, even after removing the dead pixels, the John ellipsoid corresponding to the remaining completely observed pixels in $\mathcal{X}_{\boldsymbol{\Omega}} \subseteq \mathcal{X}$ (i.e., the maximum-volume ellipsoid inside conv$\mathcal{X}_{\boldsymbol{\Omega}}$) almost remains unchanged, as can be seen in Figure 1(c).

Therefore, such approximated John ellipsoid can be used to well estimate the signatures, denoted as $\widehat{\boldsymbol{A}}$, based on which we estimate the abundances $\boldsymbol{S} = [\boldsymbol{s}_1, \ldots, \boldsymbol{s}_L]$ as follows:

- (Case 1) For a complete pixel $\boldsymbol{x}_\ell$, its abundance vector can be naturally estimated as

$$\boldsymbol{s}_\ell^\star = \arg\min_{\boldsymbol{s} \in \mathcal{T}} \|\widehat{\boldsymbol{A}}\boldsymbol{s} - \boldsymbol{x}_\ell\|_2^2, \tag{3}$$

  where $\mathcal{T} \triangleq \{\boldsymbol{s} \mid \boldsymbol{s} \in \mathbb{R}_+^N,\ \boldsymbol{1}_N^T\boldsymbol{s} = 1\}$ is the unit simplex of $\mathbb{R}^N$ that forces the abundance nonnegativity and sum-to-one constraints [15].

- (Case 2) If the ℓth pixel is incompletely acquired, then we define its support as the index set $\boldsymbol{\Omega}_\ell \triangleq \{m \mid (m, \ell) \in \boldsymbol{\Omega}\} \subseteq \mathcal{I}_M$, and hence the successfully acquired data in the ℓth pixel may be written as $[\boldsymbol{x}_\ell]_{\boldsymbol{\Omega}_\ell}$. Naturally, we estimate the abundances using the maximum available information:

$$\boldsymbol{s}_\ell^\star = \arg\min_{\boldsymbol{s} \in \mathcal{T}} \|\widehat{\boldsymbol{A}}_{\boldsymbol{\Omega}_\ell}\boldsymbol{s} - [\boldsymbol{x}_\ell]_{\boldsymbol{\Omega}_\ell}\|_2^2, \tag{4}$$

Fig. 2. False-color composition (R: 53; G: 33; B: 13) of the studied HSI subimage over Pavia Center.

  where $\widehat{\boldsymbol{A}}_{\boldsymbol{\Omega}_\ell}$ is the submatrix of $\widehat{\boldsymbol{A}}$ formed by its rows with indices in $\boldsymbol{\Omega}_\ell$.

Note that if the ℓth pixel is a complete one, we have $\boldsymbol{\Omega}_\ell = \mathcal{I}_M$, and hence (4) reduces back to (3). Therefore, we can unify the above two cases as (4), which is further regularized using sparsity prior that can improve abundance estimation as reported in [19], i.e., $\forall \ell \in \mathcal{I}_L$,

$$\boldsymbol{s}_\ell^\star = \arg\min_{\boldsymbol{s} \in \mathcal{T}} \|\widehat{\boldsymbol{A}}_{\boldsymbol{\Omega}_\ell}\boldsymbol{s} - [\boldsymbol{x}_\ell]_{\boldsymbol{\Omega}_\ell}\|_2^2 + \lambda\|\boldsymbol{s}\|_1, \tag{5}$$

where $\lambda = 0.001$ is the regularization parameter, and ℓ_1-norm (i.e., the convex envelope of the ℓ_0-norm [13]) encourages a sparse solution.

As solving (5) pixel-by-pixel is computationally inefficient as typical L is very large, we solve the L subproblems in parallel based on the following two strategies. First, by the definitions of ℓ_1-norm [13] and $\mathcal{T}$, the regularization term $\|\boldsymbol{s}\|_1$ is a constant whenever $\boldsymbol{s} \in \mathcal{T}$, making the sparsity regularization ineffective; to encourage sparse solutions, (5) is simplified as

$$\boldsymbol{s}_\ell^\star = \arg\min_{\boldsymbol{s} \in \mathbb{R}_+^N} \|\widehat{\boldsymbol{A}}_{\boldsymbol{\Omega}_\ell}\boldsymbol{s} - [\boldsymbol{x}_\ell]_{\boldsymbol{\Omega}_\ell}\|_2^2 + \lambda\|\boldsymbol{s}\|_1,\ \ \forall \ell. \tag{6}$$

Note that such simplification of leaving out the sum-to-one constraint $\boldsymbol{1}_N^T\boldsymbol{s} = 1$, not just enables the sparsity regularization, but also mitigates the nonlinear mixing effect as known in prior remote sensing literature. Second, as $N \ll M$ in practical scenarios, we have more than N completely acquired spectral bands, i.e., $|\boldsymbol{\Omega}_1 \cap \cdots \cap \boldsymbol{\Omega}_L| \geq N$, enabling approximate but efficient parallel computing of (6), namely

$$\min_{\boldsymbol{S} \in \mathbb{R}_+^{N \times L}} \|\widehat{\boldsymbol{A}}_{\boldsymbol{\Omega}_1 \cap \cdots \cap \boldsymbol{\Omega}_L}\boldsymbol{S} - \boldsymbol{X}_{\boldsymbol{\Omega}_1 \cap \cdots \cap \boldsymbol{\Omega}_L}\|_F^2 + \lambda\|\boldsymbol{S}\|_1,$$

whose solution $\boldsymbol{S}^\star$ can be computed very fast using the SUnSAL algorithm [20], where $\boldsymbol{X}_{\boldsymbol{\Omega}_1 \cap \cdots \cap \boldsymbol{\Omega}_L}$ is the submatrix of $\boldsymbol{X}$ formed by its rows with indices in the index

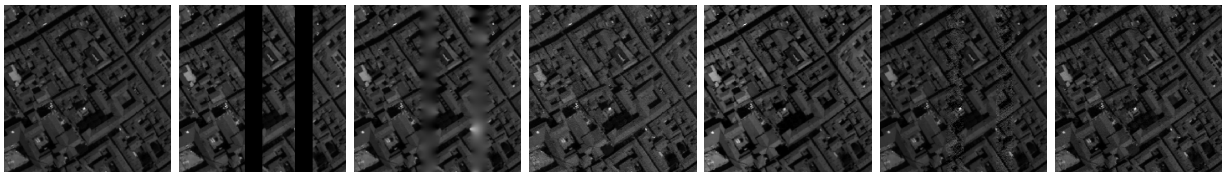

(a) (b) (c) (d) (e) (f) (g)

Fig. 3. (a) The 20th band of the studied Pavia Centre data; (b) its stripe-corrupted version. The reconstructed band image of (c) PDE, (d) UBD, (e) LLRSSTV, (f) FastHyIn, and (g) the proposed JEHI.

set $\mathbf{\Omega}_1 \cap \cdots \cap \mathbf{\Omega}_L$, and $\widehat{\boldsymbol{A}}_{\mathbf{\Omega}_1 \cap \cdots \cap \mathbf{\Omega}_L}$ is similarly defined. The reconstructed HSI is then given by $\widehat{\boldsymbol{X}} = \widehat{\boldsymbol{A}}\boldsymbol{S}^\star$. Interested readers may refer to [10] for the complexity analysis related to JE.

3. EXPERIMENTS

In this experiment, we study a widely used HSI data acquired by the Reflective Optics System Imaging Spectrometer (ROSIS) sensor over the Pavia Centre [6, 21]. The studied 200×200 subscene is displayed in Figure 2 as a false-color image. After removing some low-quality spectral bands, a total of 80 bands is used in the experiment. We investigate a highly challenging HI scenario, where 40 consecutive spectral bands of this data are corrupted by wide stripes, for simulating large incompletely acquired areas over continuous bands. The 20th band of the stripe-corrupted data and its clean version are displayed in Figures 3(b) and 3(a), respectively.

The incomplete HSI described above is then processed by several benchmark HI methods, including partial differential equations (PDE) based HI [22], UBD [3], LLRSSTV [2], FastHyIn [6] and the proposed John ellipsoid based HI (JEHI) method. JEHI is easily implementable, except for the computatio of JE that is done by the solver develped in [10] with available open source code.[2] The 20th bands of the reconstructed HSIs of these methods are displayed in Figures 3(c) to 3(g), respectively. As can be seen from Figure 3, only the proposed JEHI algorithm yield good visual quality for such a challenging HI scenario. The other methods either cannot inpaint the image or yield noisy reconstruction.

To have a better understanding, we quantitatively compare these HI methods. To measure the similarity between the 40 reconstructed bands and their reference ones, we adopt some commonly used performance metrics, including peak signal-to-noise ratio (PSNR), universal image quality index (UIQI), *erreur relative globale adimensionnelle de synthèse* (ERGAS) and spectral angle mapper (SAM). Rigorous definitions of PSNR and ERGAS can be found from [23], while that of UIQI can be found from [7]; due to space limitation, they are not recalled here. Furthermore, computational time T in seconds (sec.) is adopted as an index of computational efficiency. All the experiments in this section are executed on a computer facility equipped with Core-i7-9750H CPU with 2.60-GHz speed and 16-GB RAM, and all the HI methods are implemented in Mathworks MATLAB R2019a.

Table 1. Quantitative comparison between the proposed JEHI and other benchmark HI methods.

	PSNR	UIQI	ERGAS	SAM	T (sec.)
PDE	26.80	0.815	4.661	**2.694**	62.89
UBD	27.59	0.852	8.526	10.83	12.48
LLRSSTV	21.68	0.819	5.686	9.047	1509
FastHyIn	32.89	0.823	6.659	5.614	**6.39**
JEHI	**33.81**	**0.931**	**3.883**	5.163	25.22

The results are summarized in Table 1, where one can see that the proposed JEHI does perform best in terms of all the first three indices, while performs second w.r.t. SAM. For the global quality measure ERGAS [23], PDE and LLRSSTV also perform well. As for computational efficiency, FastHyIn and UBD are outstanding. These experimental evidences again demonstrate the essential role of the ellipsoid topology in hyperspectral analysis.

4. CONCLUSION

We have presented an unsupervised hyperspectral inpainting algorithm, termed JEHI, again showing the effectiveness of John ellipsoid in hyperspectral data analysis. John ellipsoid (i.e., the maximum-volume data-inscribed ellipsoid) has been generalized to the case of incomplete data acquisition, and is known to be robust

[2]The MATLAB code of fast JE computation is available in https://sites.google.com/view/chiahsianglin/home.

against low data purity and ill-conditioned endmember matrix. John ellipsoid holds strong endmember identifiability like the well known (non-convex) minimum-volume simplex criterion in hyperspectral remote sensing, but just requires solving a convex optimization problem bringing it another advantage in computational aspect. Experimental result has demonstrated the superiority of JEHI over benchmark HI methods.

5. REFERENCES

[1] P. Addesso, *et al.*, "Hyperspectral image inpainting based on collaborative total variation," in *Proc. IEEE International Conference on Image Processing*, Beijing, China, Sep. 2017, pp. 4282–4286.

[2] W. He, *et al.*, "Hyperspectral image denoising using local low-rank matrix recovery and global spatial–spectral total variation," *IEEE J. Sel. Top. Appl. Earth Obs. Remote Sens.*, vol. 11, no. 3, pp. 713–729, Mar. 2018.

[3] D. Cerra, *et al.*, "Unmixing-based denoising for destriping and inpainting of hyperspectral images," in *Proc. IEEE Geoscience and Remote Sensing Symposium*, Quebec City, Canada, Jul. 2014, pp. 4620–4623.

[4] C. Pan, *et al.*, "Hyperspectral image destriping using unmixing-based kriging interpolation," in *Proc. IEEE Workshop on Hyperspectral Image and Signal Processing: Evolution in Remote Sensing*, Los Angeles, USA, Aug. 2016, pp. 1–5.

[5] D. Hong, *et al.*, "An augmented linear mixing model to address spectral variability for hyperspectral unmixing," *IEEE Trans. Image Process.*, vol. 28, no. 4, pp. 1923–1938, Apr. 2019.

[6] L. Zhuang, *et al.*, "Fast hyperspectral image denoising and inpainting based on low-rank and sparse representations," *IEEE J. Sel. Top. Appl. Earth Obs. Remote Sens.*, vol. 11, no. 3, pp. 730–742, Mar. 2018.

[7] C.-H Lin, *et al.*, "An explicit and scene-adapted definition of convex self-similarity prior with application to unsupervised Sentinel-2 super-resolution," *IEEE Trans. Geosci. Remote Sens.*, vol. 58, no. 5, pp. 3352–3365, May. 2020.

[8] C.-H Lin, *et al.*, "Maximum volume inscribed ellipsoid: A new simplex-structured matrix factorization framework via facet enumeration and convex optimization," *SIAM J. Imaging Sci.*, vol. 11, no. 2, pp. 1651–1679, Jul. 2018.

[9] M. D. Craig, "Minimum-volume transforms for remotely sensed data," *IEEE Trans. Geosci. Remote Sens.*, vol. 32, no. 3, pp. 542–552, May. 1994.

[10] C.-H Lin, *et al.*, "Nonnegative blind source separation for ill-conditioned mixtures via john ellipsoid," *IEEE Trans. Neural Netw. Learn. Syst.*, pp. 1–15, Jul. 2020.

[11] C.-H Lin, *et al.*, "On the endmember identifiability of Craig's criterion for hyperspectral unmixing: A statistical analysis for three-source case," in *Proc. IEEE International Conference on Acoustics, Speech and Signal Processing*, Vancouver, Canada, May. 2013, pp. 2139–2143.

[12] C.-H Lin, *et al.*, "Identifiability of the simplex volume minimization criterion for blind hyperspectral unmixing: The no-pure-pixel case," *IEEE Trans. Geosci. Remote Sens.*, vol. 53, no. 10, pp. 5530–5546, Oct. 2015.

[13] C.-Y Chi, *et al.*, *Convex Optimization for Signal Processing and Communications: From Fundamentals to Applications*, Boca Raton, FL, USA: CRC Press, 2017.

[14] C.-H Lin, *et al.*, "Detection of sources in non-negative blind source separation by minimum description length criterion," *IEEE Trans. Neural Netw. Learn. Syst.*, vol. 29, no. 9, pp. 4022–4037, Sep. 2018.

[15] C.-H Lin, *et al.*, "A fast hyperplane-based minimum-volume enclosing simplex algorithm for blind hyperspectral unmixing," *IEEE Trans. Signal Process.*, vol. 64, no. 8, pp. 1946–1961, Apr. 2016.

[16] J. M. Bioucas-Dias, "A variable splitting augmented Lagrangian approach to linear spectral unmixing," in *Proc. IEEE Workshop on Hyperspectral Image and Signal Processing: Evolution in Remote Sensing*, Grenoble, France, Aug. 2009, pp. 1–4.

[17] "Free Samson hyperspectral data cube," [Online], Available: http://www.ehu.eus/ccwintco/index.php?title=Hyperspectral_Remote_Sensing_Scenes.

[18] F. Zhu, *et al.*, "Spectral unmixing via data-guided sparsity," *IEEE Trans. Image Process.*, vol. 23, no. 12, pp. 5412–5427, Dec. 2014.

[19] J. Chen, *et al.*, "Nonlinear estimation of material abundances in hyperspectral images with ℓ_1-norm spatial regularization," *IEEE Trans. Geosci. Remote Sens.*, vol. 52, no. 5, pp. 2654–2665, May. 2014.

[20] J. M. Bioucas-Dias, *et al.*, "Alternating direction algorithms for constrained sparse regression: Application to hyperspectral unmixing," in *Proc. IEEE Workshop on Hyperspectral Image and Signal Processing: Evolution in Remote Sensing*, Reykjavík, Iceland, Jun. 2010, pp. 1–4.

[21] "ROSIS Free Pavia Center hyperspectral data cube," [Online], Available: http://www.ehu.eus/ccwintco/index.php?title=Hyperspectral_Remote_Sensing_Scenes.

[22] J. D'Errico, "Inpainting nan elements in 3-d," MATLAB Central File Exchange. MathWorks, Natick, MA, USA, 2008, [Online], Available: https://www.mathworks.com/matlabcentral/fileexchange/21214-inpainting-nan-elements-in-3-d.

[23] C.-H Lin, *et al.*, "A convex optimization-based coupled nonnegative matrix factorization algorithm for hyperspectral and multispectral data fusion," *IEEE Trans. Geosci. Remote Sens.*, vol. 56, no. 3, pp. 1652–1667, Mar. 2018.